Instantaneous Doppler Signature Extraction from within a Spectrogram Image of a VHF Band

PIOTR PTAK
JUHA HARTIKKA
MAUNO RITOLA
TUOMO KAURANNE
Lappeenranta University of Technology
Lappeenranta, Finland

Aircraft tracking based on the Doppler shift of radio sources of opportunity presents one approach to avert or reduce tragedies like the lost flight MH370. Systems like this are based on simultaneous observation of the Doppler shift caused by aircraft from multiple common radio sources and many listeners, for example by capturing Doppler signals from spectrogram images. In the current article, a mathematical model of instantaneous Doppler curve extraction from within a VHF spectrogram image is presented and exploited with three receiving and one transmitting stations. The model is based on a priori knowledge of the probability density function (pdf) of the first-order derivative of the Doppler shift (FODDS), and on a system of blocks for identifying, classifying, and predicting the Doppler signal in a one-scan-at-a-time fashion. Tracing capabilities of such a model are tested in an off-line experiment with 21 TV signal recording sessions. The system was able to trace 73.8% of observed Doppler signatures; its stability was proven with various scenarios of Doppler curve appearance within the recorded sessions and simulated synthetic data.

Manuscript received January 31, 2015; revised July 19, 2015; released for publication September 26, 2015.

DOI. No. 10.1109/TAES.2015.150077.

Refereeing of this contribution was handled by R. Narayanan.

Authors' address: Department of Mathematics and Physics, Lappeenranta University of Technology, Skinnarilankatu 34, 53850 Lappeenranta, Finland. Corresponding author is P. Ptak, E-mail: (piotr.pawel.ptak@gmail.com).

0018-9251/16/$26.00 © 2016 IEEE

I. INTRODUCTION

Work presented in this publication is a continuation to the study on multistatic radar systems based on Doppler-only information presented in [1]. The previous paper described the principles used for aircraft tracking by passive multistatic Doppler shifts. The system was tested with very high frequency (VHF) recordings of Doppler footprints. This inverse problem of determining the location of the plane in spherical coordinates was approached by applying a mathematical model consisting of a combination of the Hough transform (HT), the Canny edge detection operator, and the secant method for minimization.

The present paper is meant to introduce a new method for extracting Doppler curves from within the image (a spectrogram matrix). The spectrogram form as a signal representation provides efficient ways of analyzing it. In [2] authors present advantages and disadvantages of different time-frequency representations in a manoeuvering air target scenario. The spectrogram representation which is pursued in this paper is designed to be quickly executable without any major loss of resolution. The method presented focuses on commercial aircraft detection, with the lost flight MH370 as a reference scenario, in which case the trajectory of the aircraft tends to follow geodesics with some minor bends. The approach used here differs from the one presented in the previous paper [1] by the instantaneous identification of Doppler curve components. The mathematical model consists mainly of cell averaging – constant false alarm rate (CA-CFAR), signal intensity analysis, and signal crossing scenario analysis.

In [3] several constant false alarm rate (CFAR) techniques suitable for over-the-horizon reception are tested. CA-CFAR is chosen over the other techniques tested in order to get good signal detection. However, in a multiple target scenario the clutter map – constant false alarm rate (CM-CFAR) or the trimmed mean – constant false alarm rate (TM-CFAR) methods would perform better in recognizing interfering targets according to these authors.

In [4] the authors present an approach to detect Doppler signatures of human movements micro–Doppler (μD) and classify them into separate categories. For feature extraction the authors proposed applying a smoothing median filter over the computed maximum power spectrum and then applying two techniques, namely a two-directional two-dimensional form of principal component analysis (2D2-PCA) and two-directional two-dimensional form of linear discriminant analysis (2D2-LDA).

The idea of detection of components within a spectrogram is a well-studied subject. Some examples involve harmonic component tracking in audio signals with a sequential Bayesian harmonic model [5], using fractional spectrograms (FS) to compute the instantaneous frequency (IF) of multicomponent nonstationary signal

[6], separation of a percussive component containing transients as an application of time-scale modification (TSM) [7], human fall detection using time-varying Doppler signatures analyzed with time-frequency representations, and matching pursuit decomposition [8]. In [6] the authors have demonstrated a method for multicomponent signal separation using an adaptive window FS provided that the local amplitudes of signal components do not vary significantly, whereas this publication presents a separation method based on separate peak recognition. This method was chosen over a maxima detection based one in a past study of extraction of frequency modulation (FM) based signal [9].

In [10] the authors demonstrate a method of reassignment (RM) in which at every time step scattered components are reallocated on a time–frequency plane to a new point that represents the distribution of energy in the time–frequency window more accurately. A special case of reassignment was introduced in [11] as a synchrosqueezing transform (SST) with the purpose of identifying speakers by incorporating a wavelet transform and auditory-nerve based models. In contrast to reassignment transform the SST allows for mode reconstruction [more efficient mode separation than empirical mode decomposition (EMD)]. A comprehensive overview of these two methods (RM and SST) is presented in [12]. In the present paper however, the components are not shifted on the plane but are rather followed as they are located with respect to their center of mass (CoM). In other words the current method allows the signal to locally fluctuate on the plane while still being trackable.

Connecting the detected components at different time instances is a well-studied subject. The Viterbi algorithm (VA) has been tested in different fields of interest [9, 13, 14]. The concept of the VA has been used in this paper, but the idea behind the current algorithm does not match fully the specifics of VA; see Section III-E.

The paper is organized as follows. After this Introduction, the second section covers the fundamentals for the ensuing analysis, which is derived from the probability density function (pdf) of the first-order derivative of Doppler shift (FODDS). The third section introduces the mathematical model developed here. In the fourth section a description of the recording circumstances and the data recorded and simulated are presented. Experimental results with the proposed model are presented in section five. Discussion of the results is presented in section six.

II. PDF OF FODDS WITH RESPECT TO VARYING SAMPLING TIME AND CRUISING VELOCITY

Let us start from the well-known bistatic Doppler shift equation presented in (1)

$$f_D(t) = \frac{f_t}{c}\frac{\mathrm{d}\left(d_{\mathrm{TA}}(t) + d_{\mathrm{A}I}(t)\right)}{\mathrm{d}t}, \tag{1}$$

where f_t represents the transmitted frequency, $d_{\mathrm{TA}}(t)$ and $d_{\mathrm{A}I}(t)$ are distances from the transmitter to an aircraft and from an aircraft to the receiver, respectively; c is the speed of electromagnetic waves, and $f_D(t)$ corresponds to the Doppler frequency (shift), $I = \mathrm{J}, \mathrm{M}$.

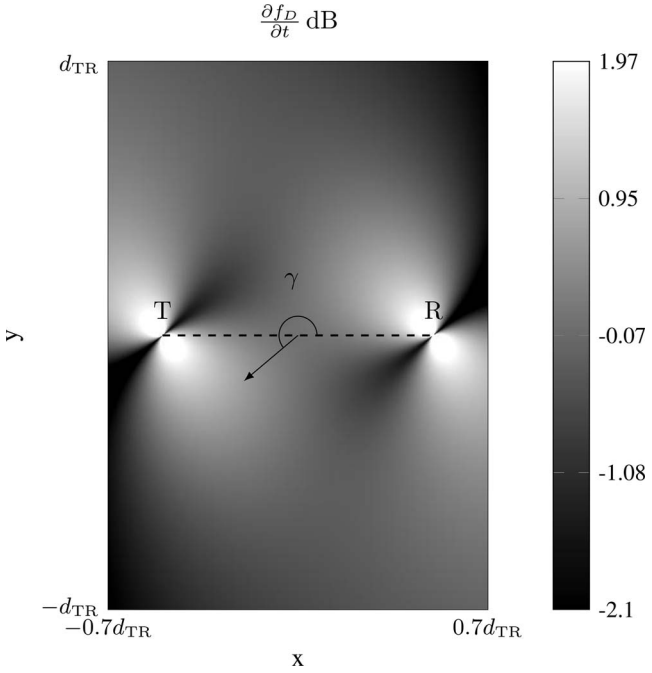

Fig. 1. Graph of first derivative of Doppler shift with respect to spatial variables x and y and constants $T = 0.5$ s, $V_c = 250$ m s^{-1}, and $\gamma = 220^\circ$.

Distances $d_{\mathrm{TA}}(t)$ and $d_{\mathrm{A}I}(t)$ from (1) can be expanded into the following form

$$d_{\mathrm{TA}}(t(1)) = \sqrt{(x - x_{\mathrm{T}})^2 + (y - y_{\mathrm{T}})^2} \tag{2}$$

$$d_{\mathrm{TA}}(t(2)) = \sqrt{(x + \Delta x - x_{\mathrm{T}})^2 + (y + \Delta y - y_{\mathrm{T}})^2} \tag{3}$$

$$d_{\mathrm{TA}}(t(3)) = \sqrt{(x + 2\Delta x - x_{\mathrm{T}})^2 + (y + 2\Delta y - y_{\mathrm{T}})^2} \tag{4}$$

where x and y are constrained to the following domain $[-0.7d_{\mathrm{TR}}, 0.7d_{\mathrm{TR}}] \times [-d_{\mathrm{TR}}, d_{\mathrm{TR}}]$, $t(3) = t(2) + T = t(1) + 2T$, d_{TR} – length of the baseline, $(x_{\mathrm{T}}, y_{\mathrm{T}})$ – transmitter location, $(x_{\mathrm{R}}, y_{\mathrm{R}})$ – receiver location, $\Delta x = V_c T \cos\gamma$, $\Delta y = V_c T \sin\gamma$. Parameter γ is an angle between the receiver-transmitter vector and the vector of the object's trajectory, measured counterclockwise; see Fig. 1. Two of the remaining parameters V_c and T are the cruising velocity and the sampling time, respectively.

Sequence $d_{\mathrm{A}I}(t(1)) \ldots d_{\mathrm{A}I}(t(3))$ has a similar construction.

Substituting the bistatic distance at time $t(p)$, $d_{\mathrm{TA}}(t(p)) + d_{\mathrm{A}I}(t(p))$ with $d_b(t(p))$ gives (1) a discretized form

$$f_D(x, y, \gamma, T, V_c) = \frac{f_t}{c}\frac{d_b(t(p-1)) - d_b(t(p))}{T} \tag{5}$$

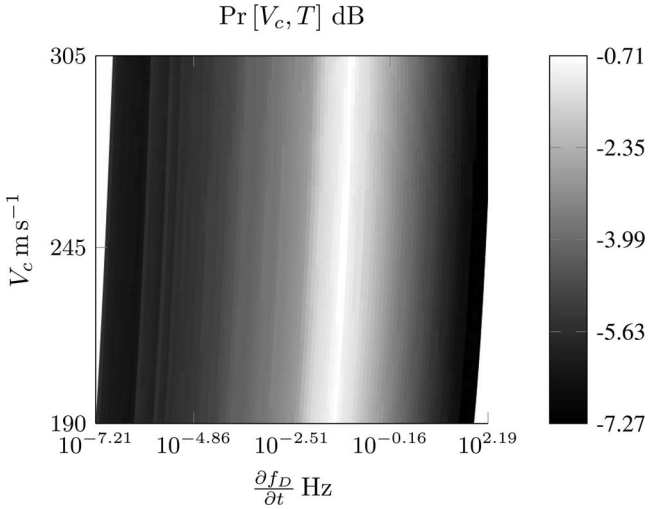

Fig. 2. Graph of pdf of FODDS value Pr [V_c, T] as function of aircraft cruising speed V_c *and* $\frac{\partial f_D}{\partial t}$.

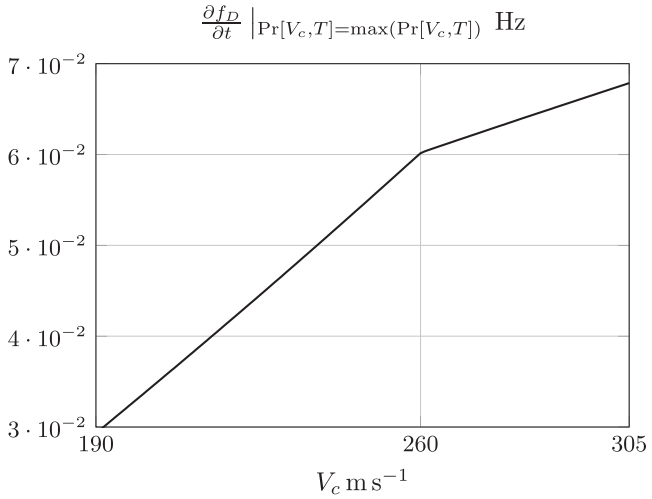

Fig. 3. FODDS as function of cruising velocity V_c for maximum observed probability.

Therefore the first derivative of (5) can be expressed as follows

$$\frac{\partial f_D(x, y, \gamma, T, V_c)}{\partial t} = \frac{f_t}{c}\left[\frac{d_b(t(p-2)) - 2d_b(t(p-1)) + d_b(t(p))}{T^2}\right] \tag{6}$$

An example of the distribution of the first derivative of the Doppler shift as a function of spatial location is presented in Fig. 1. In this case the angle γ is set to 220°, cruising velocity $V_c = 250$ m s^{-1}, and sampling time $T = 0.5$ s.

The pdf of the FODDS value as a function of cruising velocity V_c and sampling time T is expressed as

$$\Pr[V_c, T] = \int_0^{\pi}\int_{-d_{\mathrm{TR}}}^{d_{\mathrm{TR}}}\int_{-0.7d_{\mathrm{TR}}}^{0.7d_{\mathrm{TR}}} \frac{\partial f_D(x, y, \gamma, T, V_c)}{\partial t}\mathrm{d}x\mathrm{d}y\mathrm{d}\gamma \tag{7}$$

An interesting phenomenon can be observed in Fig. 2. As the cruising velocity increases, the limits of the pdf's domain (the first derivative) shift towards higher values. However the changes are not large which can be seen from Fig. 3 which demonstrates the change in the first derivative with the highest probability value over varying cruising velocity.

The graph in Fig. 4 depicts the pdf presented in (7).

III. A DOPPLER CURVE DETECTION MODEL BASED ON PDF OF FODDS

In this section a mathematical model of Doppler curve detection is presented. It is assumed that the system is incapable of tracing Doppler curves that emerge from isorange contour trajectories, or the baseline's trajectory.

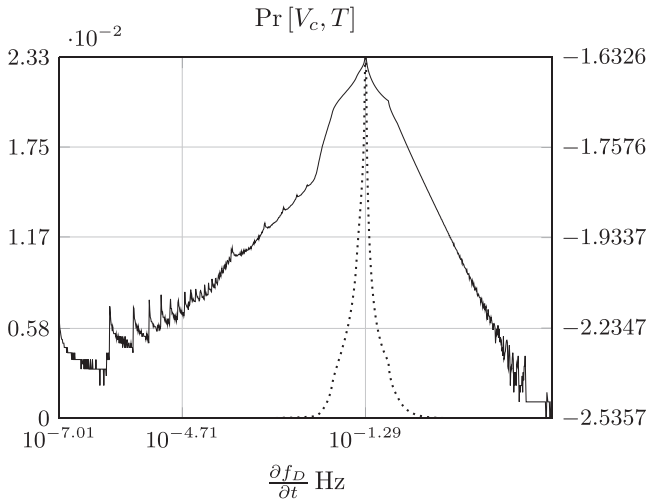

Fig. 4. PDF of FODDS. Dotted line corresponds to linear scale (left axis), solid line corresponds to logarithmic one (right axis).

The model consists of the following blocks:

1) CA-CFAR model. It is used to scan in line-by-line pattern in order to detect cells with amplitude over a certain threshold, that with some certain probability corresponds to the target echo.

2) Cells detected with CA-CFAR are analyzed to find separated peaks, defined as a group of neighboring points corresponding to the same peak, which could represent different signal sources. This step is achieved through analysis of first and second derivatives.

3) The CoM formula is applied to find the frequency that corresponds to the true maximum amplitude of each peak. The maximum-amplitude frequency points thus found are then named as the pretenders.

4) To aid prediction of the forthcoming position of signal in frequency domain we calculate the expected value of $\partial f_D(x, y, \gamma, T, V_c)/\partial t$ and denote it with $\mathrm{E}[\partial f_D/\partial t,]$; see Section III-E.

5) The classification block in which the system classifies the pretenders into separated groups which form

a logically consistent time series in a sense of Doppler shift curvature. The classification block is mainly based on a continuation of the energy concentration parameter, the distance in frequency between two consecutive steps, and probability Pr[V_c, T] of frequency difference.

6) The signal intersection block is responsible for finding cases in which two or more signals are intersecting for some period of time. It solves these cases by predicting and separating the signals based on the history of the signal's shape and amplitude.

7) The rejection block consists of the set of rules needed to reject or accept the pretenders' group.

8) The prediction block is based on a first- or second-order polynomial fit of the groups of the pretenders found, depending on the class of the signal, and on an extrapolation one step (one scan line) forth.

9) The linking block is responsible for joining two signals separated by a time gap once certain conditions are fulfilled.

Each of the listed blocks and interactions between them is presented in Fig. 5 and in the forthcoming subsections.

A. Constant False Alarm Rate

Let us denote a matrix of spectrogram data by $\mathbf{S}_{[n \times m]}$ and an amplitude of each cell of this matrix by $\mathbf{S}(t(p),\omega(j))$, where $t(p)$, $p \in [1, n]$ denotes a time for the cell being measured, and $\omega(j)$, $j \in [1, m]$ the frequency that corresponds to the cell.

The CFAR technique is well documented, and many variants of it have been developed.

As an example of this technique we want to give a brief presentation of one of the aforementioned variants, namely the CA-CFAR.

Let us consider Fig. 6 in which there are three distinguished groups of cells: reference cells (dotted), guard cells (crosshatch), and the cell under test (CUT) (grid). To check if detection is declared in the CUT we need to average over all the reference cells RC of length n_{RC} and then after multiplying it with the constant k_{CFAR} compare with the amplitude of CUT; see (8).

$$\mathbf{S}\left(t\left(k\right),\omega\left(p\right)\right) > k_{CFAR}\frac{1}{n_{RC}}\sum_{j\in RC}\mathbf{S}\left(t\left(k\right),f\left(j\right)\right), \quad (8)$$

where RC denotes a reference cell's location in the frequency domain and is of length n_{RC}, k_{CFAR} stands for a scaling constant. If the inequality is satisfied, then CUT is stored and denoted as $\mathbf{S}(t(k),\omega(p_i, t(k)))$, $p_i \in [1, m]$.

B. Grouping

The points found in the previous step are now grouped to form separate peaks of signals. This separation is achieved by examination of the frequency distance between them. If

$$\omega\left(j_i, t\left(p\right)\right) - \omega\left(j_{i+1}, t\left(p\right)\right) < f_{mr}, \quad (9)$$

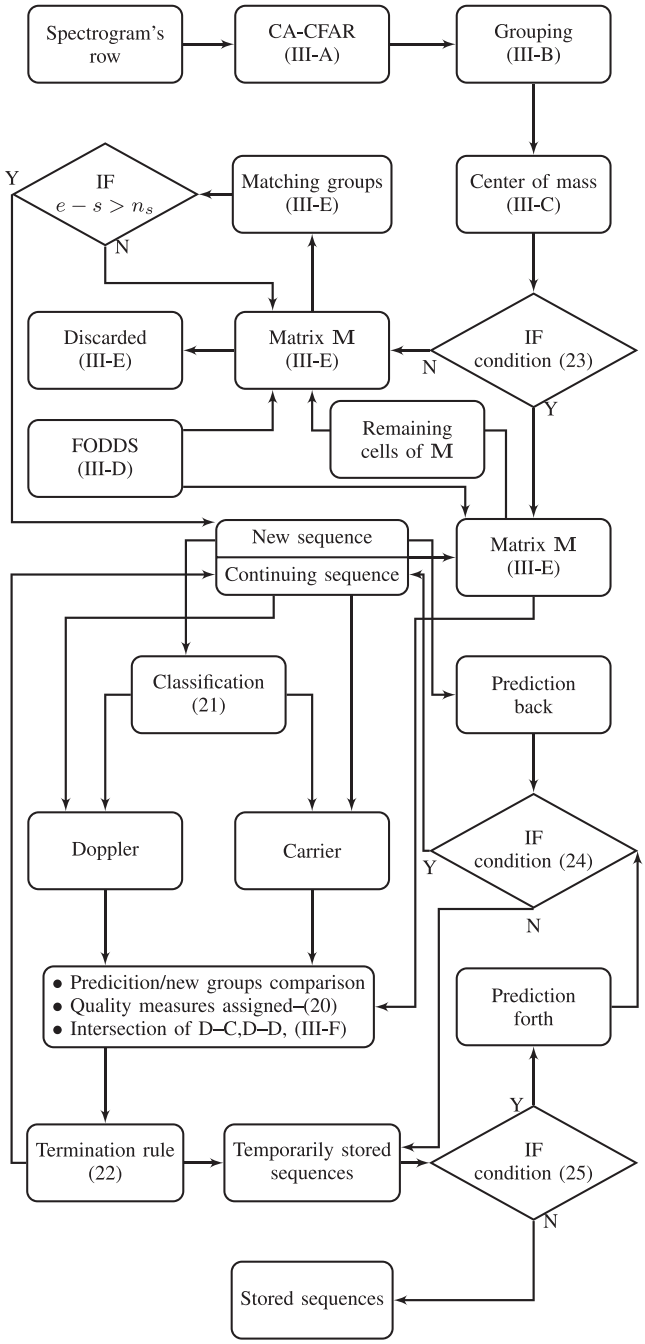

Fig. 5. Organigram of procedure presented in Section III.

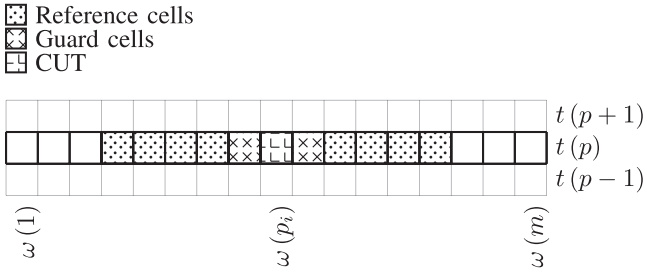

Fig. 6. CA-CFAR scheme.

where f_{mr} denotes the frequency margin between two points, then it is said that $\mathbf{S_H}$ ($t(p)$,$\omega(j_{i,}\ t(p))$) and $\mathbf{S_H}(t(p)$, $\omega\ (j_{i+1,}\ t(p))$) belong to the same group (set) $\mathbf{H}$, and $i, i+1 \in [1, |\mathbf{H}|]$, $|\mathbf{H}|$ denotes the cardinality of the group (set) $\mathbf{H}$. Further it is assumed that each group corresponds to a separated signal, both those desired to be discovered, like Doppler curves, and those originating in another source.

C. Center of Mass

The aim of this step is to find the CoM (gravity) of previously established groups. In this case mass corresponds to the amplitude of each cell $\mathbf{S_H}(t(p)$, $\omega(j_{i,}\ t(p))$) and its location is measured relative to the frequency $\omega_{\mathbf{H}}\ (j_{i,}\ t(p))$. For group $\mathbf{H}$ of cardinality equal to $b_{\mathbf{H}}$ this is achieved through the following formulae in (10) and (11).

$$\omega_l\left(t\left(p\right)\right) = \frac{1}{N_w}\sum_{i=1}^{b_{\mathbf{H}}}\left[\mathbf{S_H}\left(t\left(p\right), \omega\left(j_i, t\left(p\right)\right)\right)\omega_{\mathbf{H}}\left(j_i, t\left(p\right)\right)\right] \tag{10}$$

$$a_l\left(t\left(p\right)\right) = \mathbf{S_H}\left(t\left(p\right), w_l\left(t\left(p\right)\right)\right) \tag{11}$$

where $N_w = \sum_{i=1}^{b_{\mathbf{H}}}\mathbf{S_H}(t(p), \omega(j_i, t(p)))$. A pair $(\omega_l(t(p))$, $a_l(t(p)))$ denotes frequency and amplitude of the center for group $\mathbf{H}$ at time $t\ (p)$. The value of the amplitude refers to an interpolated value between amplitudes of two closest neighbors. The found pairs $(\omega_{l,}\ a_l)$ are then referred to as pretenders for signal carrying cells. Let us denote a number of pairs (pretenders) $(\omega_{l,}\ a_l)$ detected at time $t(p)$ as $q(t\ (p))$.

D. Expected Value

To aid the prediction of the position of a pretender in a next scan $\mathbf{S}(t(p\ +\ 1))$ we use the previously established pdf of the FODDS $\Pr[V_c, T]$. The expected value $\mathrm{E}[V_c, T]$ is used to predict the location of the next pretender for some given group $\mathbf{H}$ when there is not enough historical data (length of a set $\mathbf{S_H}(t(p)$,$\omega(j_{i,}\ t(p))$) in time domain is limited to a couple of scans) on which proper prediction could be based. Let us denote the length of the signal that is needed for predicting its next frequency value (location within frequency spectrum ω) by n_h.

E. Classification and Prediction

The classification block is the most important part of the system. It allows continuous monitoring of a previously detected pretender. The efficiency of classification depends on the quality of the signal, measured by its signal-to-noise ratio (SNR), gaps in signal reception, etc.

With every new scanned line we need to conduct a number of calculations. The first of these (12) is to check every pair of newly found pretenders and pretenders from the previous scan for their frequency differences. The resulting parameter is the first out of four that will control classification and determine how the sequence of matching pretenders eventually forms a signal. All four parameters are represented in the form of matrices,

$$\underset{\substack{l1\in[1,q(t(p-1))]\\ l2\in[1,q(t(p))]}}{\vee}\mathbf{F}_{l1,l2}(t(p)) = w_{l1}\left(t\left(p-1\right)\right) - \omega_{l2}(t(p)). \tag{12}$$

The second parameter is a result of constraining frequency differences obtained from (12), and its Boolean values $\mathbf{F}^m_{l1,l2}$ can be evaluated from (13)

$$\underset{\substack{l1\in[1,q(t(p-1))]\\ l2\in[1,q(t(p))]}}{\vee}\mathbf{F}^m_{l1,l2}\left(t\left(p\right)\right) = \left|\mathbf{F}_{l1,l2}(t(p)) < f_{mr}\right| \tag{13}$$

The next parameter determines energy concentration for each group and then checks for multiplication of energy concentration for each group from the previous step with each group from the present step. The following formula (14) represents the energy concentration value ec for group $\mathbf{H}$ of cardinality $b_{\mathbf{H}}$:

$$ec_l\left(t\left(p\right)\right) = \frac{\sum_{i=1}^{b_{\mathbf{H}}}\mathbf{S_H}\left(t\left(p\right), \omega\left(j_i, t\left(p\right)\right)\right)}{\omega_{\mathbf{H}}\left(j_{b_{\mathbf{H}}}, t(p)\right) - \omega_{\mathbf{H}}\left(j_1, t\left(p\right)\right)} \tag{14}$$

The third crucial parameter $\mathbf{EC}_{l1,l2}$ is obtained by the following formula (15).

$$\underset{\substack{l1\in[1,q(t(p-1))]\\ l2\in[1,q(t(p))]}}{\vee}\mathbf{EC}_{l1,l2}\left(t\left(p\right)\right) = ec_{l1}(t(p\ -1))\,.\ ec_{l2}\ (t\ (p)) \tag{15}$$

The fourth parameter uses knowledge on probability distribution of the FODDS

$$\underset{\substack{l1\in[1,q(t(p-1))]\\ l2\in[1,q(t(p))]}}{\vee}\mathbf{P}_{l1,l2}\left(t\left(p\right)\right) = \Pr[V_c, T]\left|\frac{\partial_{f\,D}}{\partial t}\right. = \mathbf{F}_{l1,l2}\left(t\left(p\right)\right) \tag{16}$$

Two of the aforementioned parameters are then normalized by the following equations (17), (18).

$$\underset{\substack{l1\in[1,q(t(p-1))]\\ l2\in[1,q(t(p))]}}{\vee}\mathbf{F}^s_{l1,l2}\left(t\left(p\right)\right) = \frac{1}{1+\left|\mathbf{F}_{l1,l2}\left(t\left(p\right)\right)\right|} \tag{17}$$

$$\underset{\substack{l1\in[1,q(t(p-1))]\\ l2\in[1,q(t(p))]}}{\vee}\mathbf{EC}^s_{l1,l2}\left(t\left(p\right)\right) = \frac{\mathbf{EC}_{l1,l2}\left(t\left(p\right)\right)}{\max\left(\mathbf{EC}_{l1,l2}\left(t\left(p\right)\right)\right)} \tag{18}$$

For the sake of simplicity, notations for the four established parameters are: $\mathbf{F}^s$ for normalized frequency differences matrix, $\mathbf{F}^m$ for the matrix of frequency differences in a logical form, $\mathbf{EC}^s$ for the matrix of normalized energy concentration, and $\mathbf{P}$ for matrix of the probability distribution. The four aforementioned parameters are then combined in the following fashion

$$\mathbf{M} = \mathbf{F}^s \circ \mathbf{F}^m \circ \mathbf{EC}^s + \mathbf{P} \tag{19}$$

where the operator $\circ$ denotes the Hadamard product. The newly established matrix $\mathbf{M}$ is a measure of the quality of matching between groups from the previous scan and those from the present one.

The next step is to iteratively check matrix $\mathbf{M}$ for cells with the highest values. Once the highest value has been

found, let us denote the corresponding cell with $mt_{l1,l2}$. Then the cells in the corresponding row $l1$ and column $l2$ are zeroed. In other words, this step allows only one-to-one relations between groups. This is repeated until the null matrix form is achieved.

Estimation of matrix **M** is repeated for each progressing scan. If during the process of selection by operation on matrix **M** one (or more) of the groups is consecutively chosen n_s times to have continuation in the next scan then the sequence of "matching" groups is considered as a potential signal. The sequences that do not reach the length of n_s are rejected and considered useless for further analysis. Let us denote the sequence l as $w_l(t[st, en])$, where st and en denote scan numbers when the sequence started and ended (or present scan), respectively.

Once the sequence is formed the system initializes prediction to anticipate frequency value one scan ahead. The prediction is based on the last n_h historical frequency values fitted with a second-order polynomial. In some cases the system uses a first-order polynomial; see Section III-F for details. Parameter n_h varies depending on the actual length of the sequence and can be defined as $n_h = \min\{n_s, n_{hu}\}$ where n_{hu} denotes an upper limit for the parameter n_h.

To distinguish the present quality of the signal (at time $t(p)$) it is crucial to attribute a quality measure

$$h_l(t(p)), \tag{20}$$

to a sequence l. It is done by checking if any of the newly found groups are within estimated prediction boundaries. If there exists a group that satisfies this condition then $h_l(t(p)) = 1$, if not then zero is assigned.

The sequence is then categorised into two groups, the first one corresponding to a Doppler-related signal (D) and the second one to a carrier-related signal (C). The condition for a carrier-related signal is defined in (21)

$$\left(p = n_c \wedge |p_l(t(1)) - p_l(t(p))| < f_{mc}\right) \Rightarrow w_l = w_l^c \tag{21}$$

where the pair (n_c, f_{mc}) are a length of the sequence w_l for which we check if its trend (first-order polynomial fit) p_l has deviated by f_{mc} from its starting frequency value, w_l^c denotes a newly classified sequence as a carrier (hence superscript c). The sequences that do not satisfy this condition are classified to be Doppler related.

If the signal fades out then for some time there are no recognized groups within prediction boundaries and therefore the prediction itself is used as a new estimation. In this case the assigned quality measure equals zero. If the vector of quality measure satisfies the following condition

$$\frac{1}{n_s}\sum_{i=p-n_s+1}^{p} h_l(t(i)) < p_{tr} \tag{22}$$

then the signal is terminated and temporarily stored.

F. Intersection of Sequences

This section explains the case when two or more sequences intersect on the frequency-time plane (spectrogram). Examples of intersection might involve two (or more) Doppler sequences (D-D) or Doppler and carrier sequences (D-C). In the latter case the carrier sequence tends to behave as stationary frequency-wise, but it can, and occasionally does, sway due to different equipment and weather-related causes.

For this part of the mathematical model, we assume that the sequence w_l exists

$$\bigwedge_{l\in\mathbb{Z}} \left(w_l \vee w_l^c\right) \tag{23}$$

and is longer than $n_s(en - st + 1 > n_s)$ and prediction is initialized. Among cells of matrix **M** we choose those that correspond to sequences longer than n_s. From this set we choose the one with the highest value and proceed by checking if its value is positive (>0). If that is the case then we store it for further analysis as w_l^x.

The stored sequences w_l^x are now analyzed for a possible intersection scenario. A condition that needs to be fulfilled is that two (or more) sequences share the same column of matrix **M**. In other words two (or more) sequences point at the same group as the continuation. Then depending on sequence category we use a different prediction. In the case of a Doppler signal we use a second-order polynomial to estimate the next element of the sequence; for carrier sequences we use a first-order polynomial with a significantly longer history tail on which the next element is estimated. In both cases the quality measure $h_l(t(p)) = 1$.

G. Combining Sequences

This step is important as a backup solution in a case when the system loses trace on some signal. Because a situation like that is possible we need to implement a solution for combining two curves where one of them mathematically prolongs the other one.

Every time when the new signal has been formed the system checks whether it is a continuation of any of the previous terminated signals or not. For every pair of present w_l and past w_z signals the prediction to past and prediction to future are performed, respectively, with length of prediction $n_{l,z}$ matching the time gap between them. Once the results of prediction $f_l(t[st - n_{l,z}, st - 1])$, $f_z(t[en + 1, en + n_{l,z}])$ are known the system checks the following condition:

$$\sum_{i=1}^{n_{l,z}} \omega_l(t[st - i]) - \omega_z\left(t\left[en + n_{l,z} - i + 1\right]\right) < n_{l,z} f_{mrp} \tag{24}$$

where f_{mrp} is a frequency margin for predicted values. If the condition is fulfilled then the signals are joined and the gap is complemented with values resulting from fitting the subsequences $\omega_z(t[en - n_s, en])$ and $\omega_l(t[st, st + n_s - 1])$. If the condition is not met then the system recognizes the present signal as a completely new one. Selection of

potential past signals is made based on condition of time difference

$$t_l\,(st) - t_z\,(en) < t_p, \tag{25}$$

where t_p is a time margin for the potential signal.

IV. DATA SET SPECIFICATION

A. Recorded Sessions

This section describes the data set used to demonstrate the application of the mathematical model presented in Section III.

The radio signal data (RSD) was captured by three receivers, J_1, J_2, and M located near Joensuu, Finland. Receivers J_1 and J_2 correspond to the same geographical location but different antenna configurations. A TV station located in Saint Petersburg, Russian Federation was used as a transmitter of opportunity. The receiving antennas' parameters were as follows:

1) 4-element horizontal dipole array at about 14 m above ground, with dipole end dip directed to Saint Petersburg transmitter to attenuate signal strength increase during carrier crossing, for receiver J_1,
2) rotatable horizontal 4-element 50 MHz Yagi, gain about 5 dBD, height about 7 m above ground, directive pattern typical to 5-element Yagis, for receiver J_2 and
3) long wire of 250 m, which is slightly directional to northeast and has almost similar back lobe pattern to south west, for receiver M.

The recording sessions of RSD took place on July 12, 2012 with the use of J_2 and M receivers and March 22 to April 26, 2014 with the use of J_1 and J_2 receivers.

RSD was acquired with sampling rate of 8 kHz. The receivers were tuned to record a spectrum of frequencies that includes the transmitter frequency ($f_t = 49.75$ MHz) and accompanying Doppler curves. To obtain a spectrogram form of RSD [15] the short time Fourier transform (STFT) was used with the width of a symmetrically positioned Hann window set to $L \sim 1$ s (8192 samples) and calculation time step to $G = 0.5$ s. With these settings the spectrogram is categorized as overlapped with overlapping time of ~0.5 s. This window specification ensures that information on the signal's magnitude is not lost [16]. Moreover half a second time resolution combined with 8192 samples per window provides a good time/frequency resolution for the Doppler signature of common length of tens of minutes. By studying the pdf of FODDS we can deduce that a 0.5 s window will in most cases be sufficient to ensure steady and traceable transition of Doppler signature in frequency domain, discarding some extreme cases such as aircraft trajectories passing through the baseline or nearly parallel to it.

Locations of both receiving parties that were recording RSD (J and M) and the transmitting station (T) are depicted in Fig. 7. The effective radiated power (ERP) of

Fig. 7. Geographical location of transmitter T and receivers J, M and distances between them.

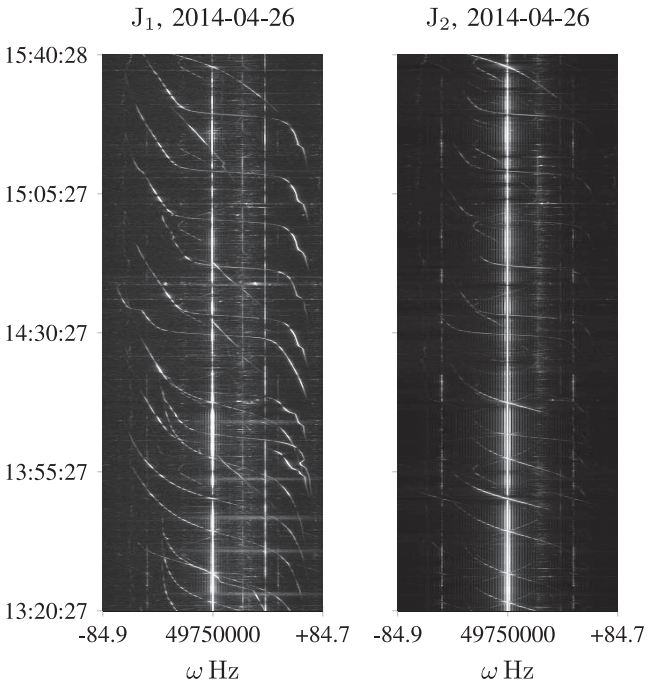

Fig. 8. Example of recorded Doppler signatures. Receivers J_1 and J_2 were tuned to receive signal from same transmitter T.

St. Peterburg's TV station used in this experiment was 149 kW.

Notable distances between receivers J, M, between the transmitter T and receivers J, M, are, respectively, $d_{JM} = 42.2$ km, $d_{TJ} = 301.8$ km, $d_{TM} = 288.4$ km.

Fig. 8 presents an example of recorded data in a form of spectrograms. In this case RSD comes from simultaneous recordings from J_1 and J_2. It is worth

TABLE I
Parameters and their Values used during Execution of the Algorithm.

Parameter	Value	Definition
k_{CFAR}	1.2	scaling constant for CA-CFAR
f_{mr}	3 Hz	frequency margin in (9)
(n_c, f_{mc})	(120 s, 1 Hz)	length of the sequence n_c for which we check if its trend (first-order polynomial fit) p_l has deviated by f_{mc} from its starting frequency value
n_{RC}	20	length of reference cells, CA-CFAR
n_{hu}	50 s	upper limit for the parameter n_h
n_s	20 s	length of sequence for which sequence is considered as a signal or length of latest values of quality measure vector
T	0.5 s	sampling time (time step)
t_p	120 s	time margin for a potential signal in combining sequences
p_{tr}	75%	termination coefficient

mentioning that the signatures received with J_1 are noticeably longer but also have a lower SNR.

B. Simulated Signal

To complement the experimental part, the synthetic Doppler signal was simulated with the help of Phased Array System Toolbox™ being a part of MATLAB™. The scenario of this simulation was suppose to imitate conditions presented in Section IV-A. The length of the baseline was set to $d_{\mathrm{TR}} = 301$ km, location of the transmitter was set at the origin (0, 0, 0), receiver's location to (0, d_{TR}, 0). Aircraft starting *st* and finishing *fi* locations were chosen randomly as $\mathrm{A}_{st}(x, y) = \{U(-0.6d_{\mathrm{TR}}, -0.2d_{\mathrm{TR}}), U(-0.2d_{\mathrm{TR}}, 1.2d_{\mathrm{TR}})\}$, $\mathrm{A}_{fi}(x, y) = \{U(0.2d_{\mathrm{TR}}, 0.6d_{\mathrm{TR}}), U(-0.2d_{\mathrm{TR}}, 1.2d_{\mathrm{TR}})\}$, and so was the altitude $alt = U$ (9750, 11270) m and the velocity $V_c = U$ (244, 257) m s^{-1}.

The transmitting frequency f_t remained the same as in the case of the St. Petersburg TV station. To obtain a different SNR of resulting Doppler signal the power of transmitted signal varied as $P_{av} = U(0, 100)$W.

The simulation involved three statistical models for the target's bistatic radar cross section (BRCS), namely: nonfluctuating, Swerling 1, and Swerling 2; additionally an ogive model was simulated and represented by system of equations (26) for ogive's BRCS [17], over which the Swerling 2 model was added to simulate smaller fluctuations.

$$\sigma_a = \begin{cases} \dfrac{\lambda^2 \tan^4\varphi \left(1-\tan^2\varphi \tan^2(\beta/2)\right)^{-3}}{16\pi \cos^3(\beta/2)}, \\ 0 \le \beta < \pi - 2\varphi \end{cases} \tag{26a}$$

$$\begin{cases} \dfrac{\pi L_o^2 (\sin(\beta/2) - \cos\varphi)}{4\sin^2\varphi \sin(\beta/2)}, \\ \pi - 2\varphi < \beta < \pi \end{cases} \tag{26b}$$

where λ, φ, β, and L_o denote wavelength, half angle, bistatic angle, and ogive's length, respectively. Additionally a rectangular signal was used as a transmitted signal. Parameters characterizing the transmitting/reflecting/receiving ends were as follows:

transmitting frequency $f_t = 49.75$ MHz
sampling frequency $f_s = 15$ kHz
pulsewidth $\epsilon = 1/1500$ s
pulse repetition frequency (PRF) $f_p = 200$ Hz
transmitter gain $G_{\mathrm{T}} = 10$ dB
preamp noise of the receiver $E_{pr} = 10$ dB
receiver gain $G_{\mathrm{R}} = 20$ dB.

Such defined signal is then transmitted, reflected from a target, received, and transformed with STFT in the same way as RSD presented in Section IV-A. Moreover parameters for the reflecting object were set:

ogive's length $L_o = 75.36$ m (A340-600 length)
ogive's half angle $\varphi = 22.5^\circ$
BRCS for nonfluctuating and Swerling 1-2 models was set $\sigma_B = 40$ m^2

V. CASE STUDY

A. Recorded Sessions

To present the performance of the method we need to list values for some of the parameters from Section III. These parameters were estimated with the use of trial data of four hours of RSD as follows:

- T, n_{RC} - sampling time and length of reference cells were set arbitrarily and the rest of the parameters were adjusted accordingly;
- k_{CFAR} - sensitivity was adaptively selected to balance ratio between discoverable signals and false alarm rate, to not inhibit detection of valid targets;
- f_{mr} - margin was decided by studying variation of width and shape over the time of a set of separate signals;
- (n_c, f_{mc}) pair was set based on analyzing the recorded Doppler signal for minimum detected change in frequency over a maximum period of time;
- n_{hu}, n_s, both parameters were decided by studying the length of unwanted signals (source other than Doppler effect or carrier).
- t_p - margin was chosen by studying length of gaps in the signal's amplitude.
- p_{tr} - sensitivity for possible termination was purposely set this high so that in the case of neighboring signals, frequency-wise, termination will prevent possible "tracing jumps" between the two signals.

The list of parameters, their values and a brief description are presented in Table I.

Testing the algorithm on the previously recorded data was divided in two stages. In the first stage, the number of visible Doppler signatures D_o on a spectrogram was counted for every recorded session with a heuristic method. This number was then used to compare with the number of properly extracted (detected) signatures D_e. The first stage also includes calculating the average time span $\bar{t}_d$ between signatures as a parameter that informs about the density of the visible Doppler curves in a given session. The second stage concentrates on the execution of the algorithm. The following parameters are gathered after analyzing each session: the number of properly extracted Doppler signatures D_e, the average signal-to-noise ratio aSNR, the number of false alarms FA. By proper extraction we mean an extraction where the length is equal to or longer than 80% of the visible curve.

Each extracted signal, besides the carrier signal, was indicated in Fig. 9. However we can notice that the carrier signal from the first image was classified as a Doppler signature because of its tendency to bend with time, therefore it remained on image. This kind of situation has been very rare and usually the carrier frequency was constant.

A number of 21 recording sessions was tested with the extraction technique presented in this paper. In Table II we have gathered variables that describe the performance of the algorithm and the measurement conditions of each session.

The presented variables are: T_s - session duration; I - receiver configuration; $\overline{t_d}$- average time gap between two consecutive Doppler signatures; D_o - number of observed Doppler signatures; D_e - number of properly extracted Doppler signatures; aSNR - average signal-to-noise ratio of the extracted signatures; FA - number of false alarms, related to CA-CFAR; FA% - percentage of false alarms s.t. $\mathrm{FA}[\%] = \frac{\mathrm{FA}}{\mathrm{FA}+D_e}$; t_e - calculation time needed for tracing the spectrogram image.

To understand the relation between parameters from Table II a correlation matrix was calculated and is presented in Fig. 10. Understanding the correlation between each pair of the parameters is a crucial step in understanding the mathematical model, therefore we treat the correlation parameter as an indicator of performance of the technique.

Examination of correlation values starts with the variable $\overline{t_d}$. The fact that it does not correlate with any of the other parameters is an indicator of the stability of the system's performance with respect to the time gap between signatures. It means that in the case of short time gaps the system manages to extract signatures at the same level of performance as in the case of longer time gaps.

The linear relation between D_o and D_e describes the stability of the model's performance measured within different recording sessions. A significant linear relation between D_o and FA and the value of the fraction D_o/FA which equals 1.95 indicate the stability of the selection technique used in the model.

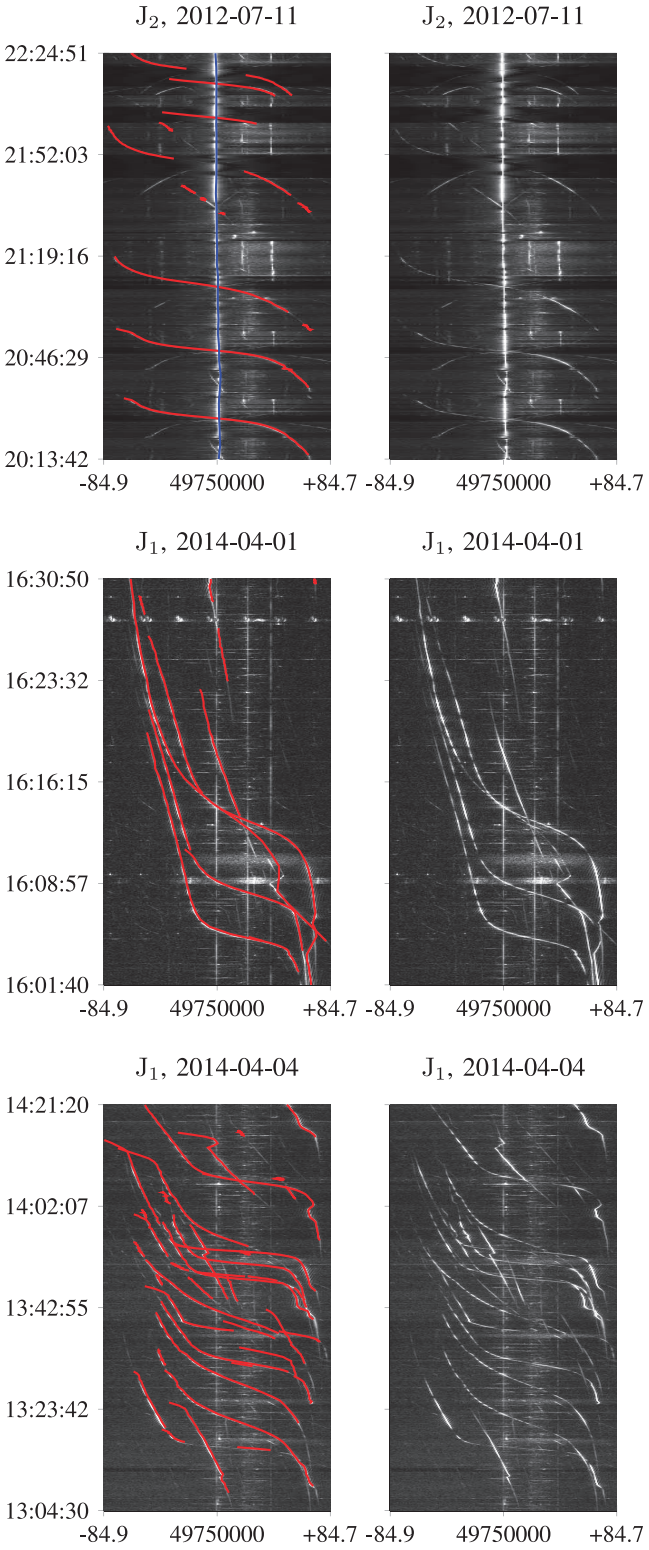

Fig. 9. Left: Result of tracing spectrogram matrix $\mathbf{S}^I$, $I = \mathrm{J}_1, \mathrm{J}_2$. Right: Image before tracing. Horizontal frequency axis expressed in Hz, vertical in wall clock units of time while recording was taken.

The relation between the detection rate D_e/D_o and the false alarm rate was found to equal –0.42 which indicates decrease in false alarm rate while increase in detected curves rate and vice versa.

TABLE II
Results of Tracing Spectrogram Images with the Presented Technique

Start	T_s	I	$\overline{t_d}$	D_o	D_e	aSNR dB	FA	FA%	t_e
2012-07-11, 20:13:42	2:11:09	J[2]	22:25	6	5	6.87	0	0	5:17
2012-07-11, 20:00:04	1:38:20	*M*	30:05	3	3	5.66	0	0	2:42
2014-03-22, 13:39:20	0:15:55	J[1]	1:55	5	3	5.77	0	0	0:39
2014-03-23, 13:16:20	0:44:20	J[1]	7:59	4	3	6.33	3	50	2:53
2014-03-27, 14:15:40	1:15:40	J[1]	6:06	11	6	5.05	10	63	4:12
2014-03-29, 13:21:20	2:30:30	J[1]	8 :51	12	9	5.06	6	40	11:09
2014-03-30, 17:52:20	1:00:50	J[1]	8:23	6	6	5.38	4	40	3:26
2014-04-01, 13:58:40	1:59:55	J[1]	6:26	15	12	6.33	9	43	8:08
2014-04-01, 16:01:40	0:29:10	J[1]	3:10	6	6	6.23	2	33	1:58
2014-04-01, 16:32:10	0:42:10	J[1]	5:13	4	3	6.22	0	0	2:32
2014-04-01, 17:21:20	1:18:42	J[1]	7:18	8	6	6.23	3	33	5:27
2014-04-02, 17:56:20	2:03:32	J[1]	8:01	13	9	6.46	4	31	7:33
2014-04-03, 13:10:00	2:22:59	J[1]	7:07	18	17	5.58	9	35	8:37
2014-04-03, 16:07:01	0:30:57	J[1]	2:50	5	3	6.31	1	25	1:37
2014-04-04, 11:39:00	0:38:38	J[1]	3:22	2	2	4.62	0	0	1:31
2014-04-04, 13:04:30	1:16:44	J[1]	4:27	14	13	5.64	2	13	3:54
2014-04-04, 17:10:30	1:51:35	J[1]	8:08	16	13	5.62	5	28	5:38
2014-04-05, 12:50:50	2:33:19	J[1]	8:28	17	12	5.55	11	33	10:36
2014-04-07, 13:18:30	2:16:30	J[1]	5:40	20	14	5.55	12	46	8:02
2014-04-26, 11:29:02	4:11:48	J[1]	9:39	20	11	5.63	14	54	17:12
2014-04-26, 11:29:02	4:11:48	J[2]	9:54	17	8	8.18	19	70	16:38
				222	**164**	**5.88**	**114**	**41**	

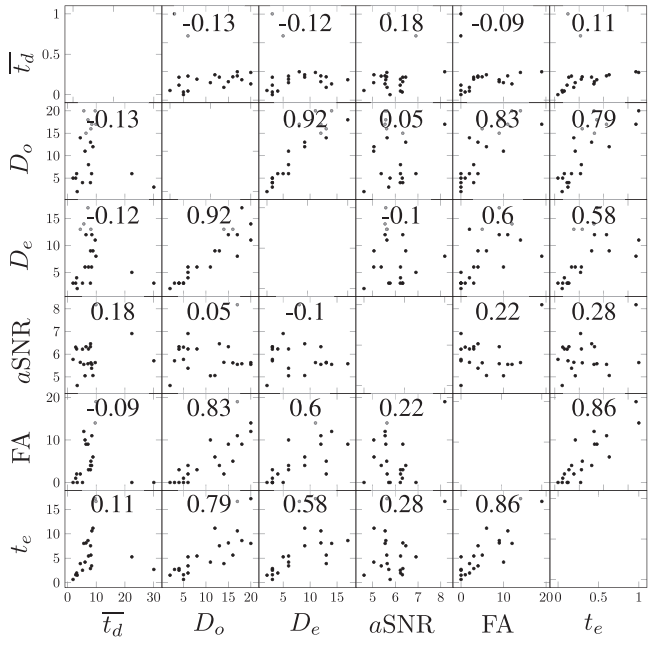

Fig. 10. Pairwise correlation plot between variables presented in Table II.

It was found that there is no correlation between aSNR and any other parameter, which at that stage of analysis is challenging to interpret.

Finally, there is a very significant correlation between the time t_e and FA which confirms the linearity of the model.

The efficiency of the system was found to equal $D_e/D_o = 73.8\%$.

B. Simulated Signal

The tests in this subsection were conducted with simulated data introduced in Section IV-B. To check the quality of signature extraction of the algorithm, the same parameter values presented in Table I that were used to test the real signal, were used.

Results presented in this section are based on 1400 simulations with varying parameters A_{st} (x, y), A_{fi} (x, y), *alt*, V_c, P_{av} and randomly chosen statistical model. During each simulation the exact location of the Doppler signature on the time-frequency plane was known based on (1). The exact Doppler was then stored as $(f_D, a_o, t), f_D\ (t), a_o(t, f_D)$, where t denotes time instances of Doppler signature, f_D the frequency values, and a_o amplitude values (SNR dB). Moreover the extracted signatures were stored in a form of $(\omega_l, a_l, t\ [st, en])$, $\omega_l\ (t)$, $a_l\ (t, \omega_l)$ where $t[st, en]$ denotes time instances over which the extraction was successful, ω_l the frequency values, and a_l amplitude values of the extraction (SNR dB). The amplitude values of the extracted signature were averaged over time t $[st, en]$ so that each signature was indicated by its averaged SNR aSNR.

To compare the efficiency of the system on the set of statistical models the ratio r_e between lengths of extraction time t $[st, en]$ and exact Doppler time length t was calculated as $r_e = \frac{t[st,en]}{t}$. Dependency of r_e as a function of aSNR is shown in Fig. 11. Scattered values were fitted with a third-order polynomial (TOP) (red solid curves in Fig. 11) and compared for every model in Fig. 12 together

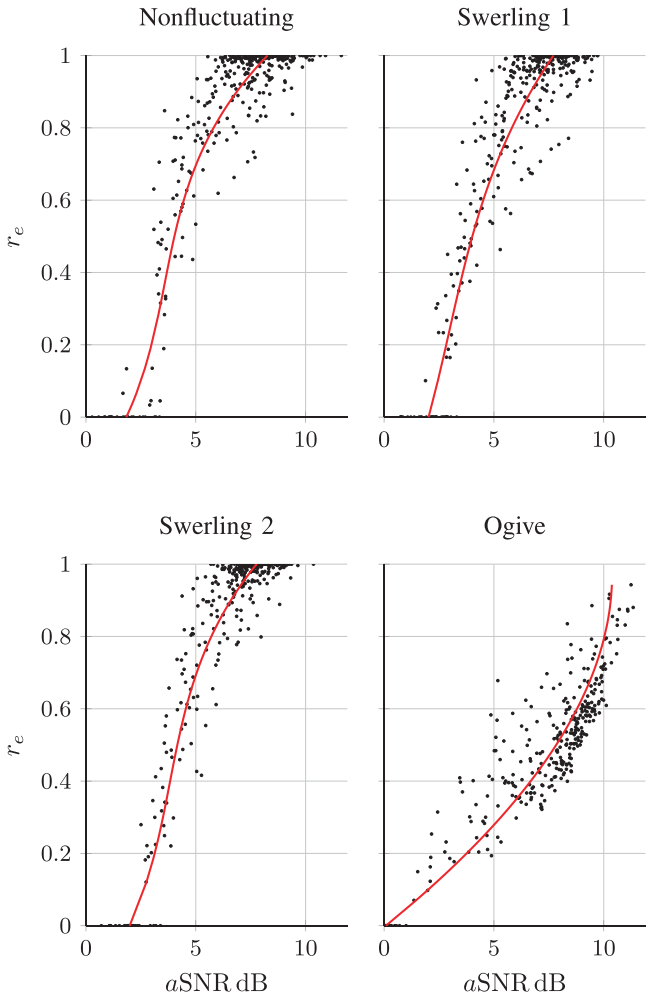

Fig. 11. Extraction time to exact Doppler time ratio r_e as function of aSNR (averaged SNR over extracted time length $t\,[st, en]$) for three statistical models and an ogive.

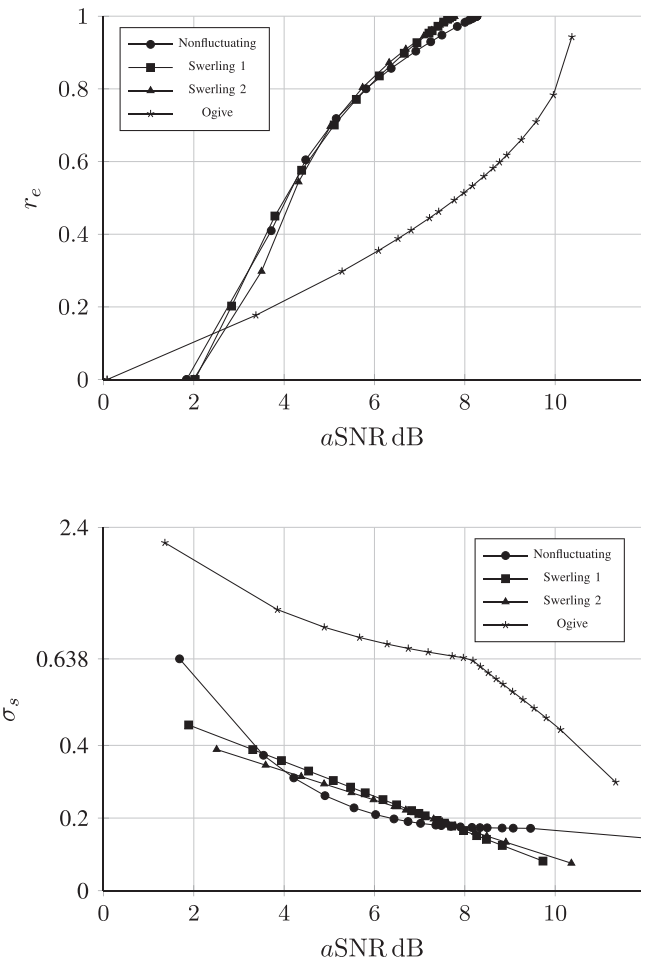

Fig. 12. Ratio r_e as function of aSNR (top figure) and standard deviation of difference $f_D\,(t\,[st, en]) - \omega_l\,(t\,[st, en])$ as function of aSNR (bottom figure). Note change of scale for ogive model [0.638, 2, 4].

with the standard deviation of difference

$$\sigma_s = \frac{1}{t\,(en) - t\,(st)} \sum_{t[st,en]} \left[f_D\,(t\,[st, en]) - \omega_l\,(t\,[st, en]) \right]^2 \tag{27}$$

The standard deviation values were fitted with a TOP for the nonfluctuating and ogive models, the rest (Swerling 1-2) were equipped with fitted lines. Note that the scale of the right figure was changed for the ogive curve ([0.638, 2.4]).

An overall performance of the system with simulated data can be expressed with an average value of the parameter r_e which was equal to $\overline{r_e}$= [0.82, 0.77, 0.81, 0.47] for nonfluctuating, Swerling 1, 2, and ogive, respectively. The averaged values of σ_s for the aforementioned models were $\overline{\sigma_s}$ = [0.21, 0.23, 0.22, 0.74] Hz. The values of $\overline{r_e}$ for three first models indicate a good performance of the algorithm, but the relatively smaller value for the fourth one is caused by the fact that an ogive was detectable mainly when the case (26b) was in use ($\pi - 2\varphi < \beta < \pi$). Average standard deviation $\overline{\sigma_s}$ values do not exceed a frequency resolution in the time-frequency plane which equals ~0.91 Hz.

It is worth noting that the algorithm is able to separate between two or more intersecting signals – the system recognizes them and follows the curves separately, as illustrated in Fig. 13, which in that respect is an advantage over an algorithm presented in [9]. The experiment with two targets was conducted under the same conditions as defined earlier in Section IV-B with transmitting power $P_{av} = 25$ W which resulted in aSNR = 5.39 dB. The intersection does not influence the quality of extraction frequency-wise and there is no significant alternation of trend of σ_s; see right illustration in Fig. 13.

VI. DISCUSSION

This work is devoted to establishing a novel method of instantaneous Doppler signature extraction from within VHF band spectrogram images. We establish a pdf of the FODDS. This pdf is used for estimating the expected value and therefore the expected frequency shift. The

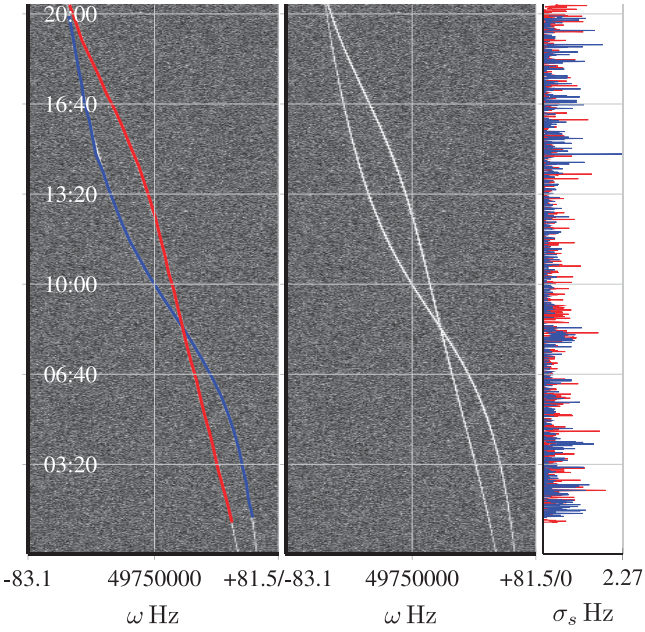

Fig. 13. Extraction of two targets. Left: extracted features; center: simulated spectrogram; right: standard deviation of frequency differences σ_s between extracted signatures and exact signatures. Vertical axes represent wall clock time [MM:SS].

structure of the mathematical model consists of a number of blocks, the most relevant of which are:

1) a CA-CFAR block responsible for detection of amplitude-wise outlying cells;
2) construction of pretenders based CoM on formulae;
3) classification of pretenders which uses signal energy concentration and frequency difference between two consecutive steps and pdf of FODDS;
4) the case of intersection of multiple signals is solved by predicting the signals' location in the frequency domain;
5) a block of combining signals is responsible for linking two signals into one across a time gap between them and a distance gap between their predicted frequency values. The missing link is then created by extrapolating with a second-order polynomial based on the number of points from the proper ends of both signals.

Based on 21 recording sessions that were tested with the technique developed in this paper we observed a 73% efficiency in extracting Doppler signatures, while in the case of the synthetic signal an efficiency of [0.82, 0.77, 0.81, 0.47] was achieved for nonlinear, Swerling 1, 2, and ogive test signals, respectively. This fact, combined with the possibility in which many more transmitter-receiver pairs are used, may establish a system like the one described in [1] with which hopefully no civilian large aircraft is untraceable when the receivers work together in a multistatic configuration.

REFERENCES

[1] Ptak, P., Hartikka, J., Ritola, M., and Kauranne, T.
Long-distance multistatic aircraft tracking with VHF frequency Doppler effect.
IEEE Transactions on Aerospace and Electronic Systems, **50**, 3 (July 2014), 2242–2252.

[2] Thayaparan, T., and Kennedy, S.
Detection of a manoeuvring air target in sea-clutter using joint time-frequency analysis techniques.
IEE Proceedings - Radar, Sonar and Navigation, **151**, 1 (Feb. 2004), 19–30.

[3] Xiangwei, M., Jian, G., and You, H.
CFAR techniques for over-the-horizon radar.
In *Proceedings of 2003 IEEE International Symposium on Intelligent Signal Processing*, Sept. 2003, 83–85.

[4] Li, J., Phung, S. L., Tivive, F., and Bouzerdoum, A.
Automatic classification of human motions using Doppler radar.
In *Proceedings of the 2012 International Joint Conference on Neural Networks (IJCNN)*, June 2012, 1–6.

[5] Dubois, C., and Davy, M.
Joint detection and tracking of time-varying harmonic components: A flexible Bayesian approach.
IEEE Transactions on Audio, Speech, and Language Processing, **15**, 4 (May 2007), 1283–1295.

[6] Khan, N., and Boashash, B.
Instantaneous frequency estimation of multicomponent nonstationary signals using multiview time-frequency distributions based on the adaptive fractional spectrogram.
IEEE Signal Processing Letters, **20**, 2 (Feb. 2013), 157–160.

[7] Driedger, J., Muller, M., and Ewert, S.
Improving time-scale modification of music signals using harmonic-percussive separation.
IEEE Signal Processing Letters, **21**, 1 (Jan. 2014), 105–109.

[8] Wu, M., Dai, X., Zhang, Y., Davidson, B., Amin, M., and Zhang, J.
Fall detection based on sequential modeling of radar signal time-frequency features.
In *Proceedings of 2013 IEEE International Conference on Healthcare Informatics (ICHI)*, Sept. 2013, 169–174.

[9] Djurović, I., and Stanković, L.
An algorithm for the Wigner distribution based instantaneous frequency estimation in a high noise environment.
Signal Processing, **84**, 3 (2004), 631–643. [Online]. Available: http://www.sciencedirect.com/science/article/pii/S0165168403003463

[10] Plante, F., Meyer, G., and Ainsworth, W.
Improvement of speech spectrogram accuracy by the method of reassignment.
IEEE Transactions on Speech and Audio Processing, **6**, 3 (May 1998), 282–287.

[11] Daubechies, I., and Maes, S.
A nonlinear squeezing of the continuous wavelet transform based on auditory nerve models.
In *Wavelets in Medicine and Biology*, 1st ed. Boca Raton, FL: CRC Press, 1996, pp. 527–546.

[12] Auger, F., Flandrin, P., Lin, Y.-T., McLaughlin, S., Meignen, S., Oberlin, T., and Wu, H.-T.
Time-frequency reassignment and synchrosqueezing: An overview.
IEEE Signal Processing Magazine, **30**, 6 (Nov. 2013), 32–41.

[13] Hara, S., Wannasarnmaytha, A., Tsuchida, Y., and Morinaga, N.
A novel FSK demodulation method using short-time DFT analysis for LEO satellite communication systems.
IEEE Transactions on Vehicular Technology, **46**, 3 (Aug. 1997), 625–633.

[14] Ochiai, H.
A novel trellis-shaping design with both peak and average power reduction for OFDM systems.
IEEE Transactions on Communications, **52**, 11 (Nov. 2004), 1916–1926.

[15] Bracewell, R.
The Fourier Transform and Its Applications
(Electrical engineering series).
New York: McGraw Hill, 2000. [Online]. Available: http://books.google.no/books?id=ZNQQAQAAIAAJ.

[16] Izraelevitz, D.
Some results on the time-frequency sampling of the short-time Fourier transform magnitude.
IEEE Transactions on Acoustics, Speech and Signal Processing, **33**, 6 (Dec. 1985), 1611–1613.

[17] Siegel, K., Alperin, H., Bonkowski, R., Crispin, J., Maffett, A., Schensted, C., and Schensted, I.
Bistatic radar cross sections of surfaces of revolution.
Journal of Applied Physics, **26**, 3 (Mar. 1955), 297–305.

Piotr Ptak received his M.Sc. degree in applied mathematics from University of Zielona Góra, Poland, in 2004 and a second M.Sc. degree in information technology from Lappeenranta University of Technology, Finland in 2006. He received his doctoral degree, approved with distinction, from Lappeenranta University of Technology in 2015.

He has been involved in a number of different research and editorial projects since 2006. His research interests include tracking of airborne objects, Doppler-only tracking systems, analysis and forecast of spot market prices and inverse problems.

Since 2007 Dr. Ptak is a co-editor of *Journal of European Consortium for Mathematics in Industry*.

Juha Hartikka received his M.Sc. degree in mechanical engineering from Lappeenranta University of Technology, Finland in 1986.

His interests include research in a field of wave propagation in electrosphere, prediction of time span for introduction and utilization of new technologies, aircraft radio scatter. Among his experiments for Quantuum Electric Ltd., one can find capacitive motor experiments which led to finding an explanation for operation of capacitive insulator type electrostatic motors, by means of capacitive effect of surface charge voltage and electrostatic force amplification.

Mauno Ritola studied radio communication and broadcasting in Leningrad Institute of Radiocommunication and Broadcasting, Russian Federation in 1979–1981. He received the M.Sc. (B.A.) with economic geography as major from Turku School of Economics and Business Administration, Finland in 1990.

For the last 10 years he has been working in monitoring for reception and frequency planning for the International Broadcasting Bureau and co-editor for the World Radio TV Handbook. He has had radio reception as his hobby for over 40 years.

Tuomo Kauranne is the founder and President of Arbonaut Ltd. since 1994. He is also Associate Professor in Applied Mathematics at Lappeenranta University of Technology, Finland. Arbonaut Ltd. is a technology company based in Joensuu, Finland that conducts forest resource mapping via remote sensing methods on six continents, and integrates geographical information systems for forest sector organizations.
Dr. Kauranne's research interests include airborne and space-borne remote sensing and mathematical modelling of geophysical, ecological, and economic processes.